Crystallographic Studies of Xe and Kr Binding within the Large Internal Cavity of Cytochrome ba_3 from *Thermus thermophilus*: Structural Analysis and Role of Oxygen Transport Channels in the Heme−Cu Oxidases[†,‡]

V. Mitch Luna, Ying Chen, James A. Fee,* and C. David Stout*

Department of Molecular Biology, The Scripps Research Institute, 10550 North Torrey Pines Road, La Jolla, California 92037

Received January 9, 2008; Revised Manuscript Received February 28, 2008

ABSTRACT: Cytochrome ba_3 is a cytochrome *c* oxidase from the plasma membrane of *Thermus thermophilus* and is the preferred terminal enzyme of cellular respiration at low dioxygen tensions. Using cytochrome ba_3 crystals pressurized at varying conditions under Xe or Kr gas, and X-ray data for six crystals, we identify the relative affinities of Xe and Kr atoms for as many as seven distinct binding sites. These sites track a continuous, Y-shaped channel, 18–20 Å in length, lined by hydrophobic residues, which leads from the surface of the protein where two entrance holes, representing the top of the Y, connect the bilayer to the a_3−Cu_B center at the base of the Y. Considering the increased affinity of O_2 for hydrophobic environments, the hydrophobic nature of the channel, its orientation within the bilayer, its connection to the active site, its uniform diameter, its virtually complete occupation by Xe, and its isomorphous presence in the native enzyme, we infer that the channel is a diffusion pathway for O_2 into the dinuclear center of cytochrome ba_3. These observations provide a basis for analyzing similar channels in other oxidases of known structure, and these structures are discussed in terms of mechanisms of O_2 transport in biological systems, details of CO binding to and egress from the dinuclear center, the bifurcation of the oxygen-in and water-out pathways, and the possible role of the oxygen channel in aerobic thermophily.

Cytochrome ba_3 (ba_3)[1] is a divergent member of the integral-membrane, heme−copper oxidase superfamily of respiratory enzymes, which function as terminal oxidases for aerobic metabolism. By reducing O_2 to H_2O and maintaining the proton gradient across the plasma membrane, these enzymes contribute to the energy needs of the cell (*1*). *Thermus thermophilus* HB8 grows in the range of 60 to ∼85 °C (*2*) and, at oxygen concentrations of ∼10 μM, utilizes cytochrome ba_3 as the preferred respiratory enzyme (*3*). The overall reaction catalyzed is

$$4\text{cyt } c^{2+} + O_2 + 8H^+_{in} \rightarrow 4\text{cyt } c^{3+} + 2H_2O + 4H^+_{out} \quad (1)$$

where in and out refer to the internal space and the periplasmic or intermenbrane space of the bacterial cell or the mitochondrion, respectively.

X-ray crystal structures exist for bovine cytochrome aa_3 [Protein Data Bank (PDB) entry 1OCC] (*4*), *Paracoccus denitrificans* (*Pd*) aa_3 (PDB entry 1AR1) (*5*), *Rhodobacter sphaeroides* (*Rs*) aa_3 (PDB entries 1M56 and 2GSM) (*6, 7*), and *T. thermophilus* HB8 (*Tt*) cytochrome ba_3 (PDB entries 1EHK and 1XME) (*8, 9*), all of which are cytochrome *c* oxidases, and *Escherichia coli* (*Ec*) bo_3 which is a quinol oxidase that lacks the Cu_A center (PDB entry 1FFT) (*10*). Combined with complementary spectroscopic studies over the past several decades, it is well-established that a six-coordinate heme is low-spin in both ferric and ferrous valence states while a heme in the proximity of Cu_B is high-spin in both ferric and ferrous valences. Electrons typically enter the enzyme from a cytochrome *c* to the Cu_A site and migrate from there to the low-spin heme and subsequently to the dinuclear center.

Dioxygen reduction occurs at the high-spin, heme a_3−Cu_B dinuclear center (dnc) (*11*). The electron transfer steps and the intermediates formed during dioxygen reduction have been widely studied in several of the heme−Cu oxidases (*12*). In contrast, rather little is known about pathway(s) via which O_2 arrives at the heme a_3−Cu_B center, which is deeply buried within the transmembrane domain of these enzymes.

Cavities and packing defects are commonly observed in the interiors of folded proteins (for relevant studies, see ref *13* and references therein). In these cases, hydrophobic cavities have been identified using xenon gas as a probe, pressurized protein crystals, and X-ray crystallography (*14*). As first applied to myoglobin, this technique revealed multiple Xe atoms at variable occupancies within hydrophobic cavities and channels, proposed to function as pathways for O_2 to the heme (*15*). Krypton can also be used for the same purpose, although it does have a lower affinity for hydrophobic sites (*16*). Properties of Xe and Kr make

[†] This work was supported by National Institutes of Health Grant GM 35342.

[‡] The coordinates and observed structure factor amplitudes for the structure with the most resolved xenon sites (100 psi, 5 min) have been deposited in the Protein Data Bank as entry 3BVD.

* To whom correspondence should be addressed. J.A.F.: telephone, (858) 784-9235; e-mail, jafee@scripps.edu; fax, (858) 784-2857. C.D.S.: telephone, (858) 784-8738; e-mail, dave@scripps.edu; fax, (858) 784-2857.

[1] Abbreviations: ba_3, cytochrome ba_3 oxidase; *Pd*, *Paracoccus denitrificans*; *Rs*, *Rhodobacter sphaeroides*; *Tt*, *Thermus thermophilus*; *Ec*, *Escherichia coli*; dnc, dinuclear center; a_3−Cu_B center, heme a_3−Cu_B enzymatic center.

10.1021/bi800045y CCC: $40.75
Published on Web 04/01/2008

them particularly good analogues of O_2; each gas favors solubility in hydrophobic environments (*17*), and the van der Waals diameters of Xe (~4.3 Å) and Kr (~4.0 Å) (*18*) are similar to that of O_2 (~4.2 Å along the O−O bond) (*19*). (When the atoms are treated as spheres, the van der Waals surface areas of Xe, Kr, and O_2 are 58, 50, and 55 Å^2 and the van der Waals volumes 42, 34, and 39 Å^3, respectively.) Xe and Kr have also been used as heavy atoms in crystallographic experiments (*14*) where the inert gas atoms may bind at adventitious sites or act as mimics of other gaseous substrates (*16*).

On the basis of their crystal structures, O_2 pathways have been suggested in bovine heart, *Pd*, *Rs*, and *Tt* cytochrome *c* oxidases (*4, 5, 20*) and in *Ec* bo_3 (*10*). Experiments with *Pd* aa_3 and *Ec* bo_3, using biochemical techniques and mutagenesis, have shown the proposed pathways are indeed functional channels for O_2 diffusion (*21*). At present, only the *Rs* enzyme has been probed with noble gas pressurization. In the latter case, two hydrophobic Xe binding sites were identified, defining part of a possible track from the membrane-facing protein surface to the active site (*7*), and following a somewhat different course than originally proposed (*20*). In this paper, we present crystallographic evidence for the presence of a continuous, hydrophobic channel from two entrances within the lipid bilayer to the heme a_3−Cu_B center in ba_3, using the method of noble gas pressurization. The analysis provides insight into the mechanism of O_2 transport, diffusion, and consumption in cytochrome *c* oxidases.

EXPERIMENTAL PROCEDURES

Protein Purification and Crystallization. Robust crystals of ba_3 are necessary to survive the noble gas pressurization procedure. The double mutant (I-K258R and II-E4Q) of ba_3 reproducibly forms large single crystals within 1–3 days (*22*). The protein was expressed and purified as previously described (*23*) and exchanged into the crystallization buffer [10 mM bis-Tris (pH 7.0), 100 mM KCl, and 13 mM nonyl β-D-glucopyranoside] using the procedure developed by Hunsicker-Wang and colleagues (*8*). Three days prior to available beam time at the Stanford Synchrotron Radiation Laboratory (SSRL), crystallization experiments were set up at SSRL using the vapor diffusion method and reservoir solutions containing 12–17% PEG 2000 and 15–60 mM bis-Tris (pH 7.0) (*8, 9*). Incubation overnight at 297 K yielded large single crystals of ba_3 with properties previously described (*22*).

Noble Gas Pressurization. Xenon and krypton derivatives were produced at room temperature by pressurizing crystals of ba_3 using the SSRL pressurization cell developed and used by Soltis and co-workers (*14*). For Xe or Kr gas pressurization, a crystal was mounted in a nylon loop from the mother liquor, dipped through cryoprotectant (100% paraffin oil), and placed in the pressure vessel. Following incubation (5–20 min), the pressure was released (5–10 s) and the crystal was flash-frozen by being plunged into liquid nitrogen. Multiple pressures (100–300 psi) were tested in combination with the range of incubation times; approximately 30 crystals were individually screened for diffraction. Eleven complete data sets were collected, and six were used for analyses of Xe and Kr positions (Table 1).

Data Collection and Structure Determination. All data sets were collected on SSRL beam line 9-1 using $\lambda = 0.979$ Å or $\lambda = 0.865$ Å radiation (Table 1). Data were recorded with an ADSC Q315 CCD detector, integrated with MOSFLM (*24*), and scaled using SCALA (*24, 25*). Molecular replacement was conducted with MOLREP (*25*) using the wild-type recombinant structure of ba_3 (PDB entry 1XME) as a search model. Model rebuilding and refinement were conducted using COOT (*26*) and REFMAC5 (*27*), respectively. TLS motion (translation, libration, screw) describes flexibility in protein structures in terms of motions of groups of residues or domains. Parameters for TLS refinement of ba_3 in the Xe- and Kr-pressurized crystals were derived from the higher-resolution (2.4 Å) structure (PDB entry 1XME) using the TLSMD server (*28*). The TLS groups were used in REFMAC5 protein refinement to derive an overall *B* value for the Xe- and Kr-pressurized crystals, which were subsequently used for heavy atom occupancy refinement (below). Following rigid body refinement of the 1XME protein model against each data set, Xe or Kr sites were identified using $2|F_o| - |F_c|$ and $|F_o| - |F_c|$ electron density maps. Atomic coordinates of the Xe and Kr atoms were then refined against the largest anomalous differences [$\geq 6.0\sigma(\Delta F)$, where $\Delta F = |F^+| - |F^-|$] for each data set using CNS (*29*). Fe and Cu atoms were included but were fixed at the coordinates derived from protein refinement. Anomalous scattering factors for Kr were determined from X-ray absorption scans recorded at beam line 9-1 using Blu-ice hutch control software (*30*); anomalous scattering factors for Fe, Cu, and Xe were taken from tables for the wavelengths that were used. Finally, with Xe and Kr positional coordinates refined, the occupancies of the Xe and Kr sites were refined against the complete anomalous difference data sets using CNS. In these calculations, Fe and Cu occupancies were fixed at 1.0, and the protein model was treated as a rigid body. Data collection and refinement statistics are summarized in Table 1.

Computational Analyses. Primary sequence alignment was done using CLUSTALW (*31*); secondary structure alignment was done using SEQUOIA (*32*). VOIDOO (*33*) was used to define the channels (cavities) in each of the four cytochrome *c* oxidase structures that was analyzed, and to calculate cavity volumes (grid size, 0.50 Å; probe sizes, 0.75–1.4 Å). FLOOD (*33*) was used to assess the maximum number of Xe atoms able to occupy the hydrophobic channels.

RESULTS

When the method of Xe gas pressurization was applied to cytochrome ba_3 crystals, up to seven Xe binding sites are observed (Figure 1A,B). Five data sets were used for occupancy refinement of Xe positions, and one was used for Kr positions, reflecting varying incubation times and pressures (Table 1). Five sites are major, being present in all data sets, while two additional minor sites are observed for the 3.37 Å resolution data set. The degree of uncertainty from occupancy refinement is difficult to assess, but the generally consistent ranking in five refinements suggests it is approximately ±10%. The top two sites are the most occupied in four of five Xe data sets. Kr, with its smaller van der Waals diameter, shares five of seven Xe sites, but overall, Kr binds less well under comparable pressurization conditions.

Table 1: Crystallographic Statistics

	Condition					
noble gas	Xe	Xe	Xe	Xe	Xe	Kr
pressure (psi)	100	200	200	200	300	300
time (min)	5	5	10	20	10	10
	Data Collection					
wavelength (Å)	0.979	0.979	0.979	0.979	0.979	0.865
resolution (Å)	3.37	3.90	4.04	3.69	3.40	3.28
no. of measured reflections	74282	28192	31170	30249	41409	69644
no. of unique reflections	16341	10269	8880	11633	14216	14810
redundancy	4.5	2.7	3.5	2.6	2.9	4.7
completeness (%)	99.7 (100.0)[a]	96.8 (91.3)[a]	97.1 (97.6)[a]	96.7 (98.1)[a]	90.7 (77.8)[a]	85.7 (63.5)[a]
$\langle I\rangle/\langle\sigma_I\rangle$	9.2 (1.8)[a]	8.5 (1.5)[a]	6.6 (1.6)[a]	7.9 (2.3)[a]	10.0 (1.4)[a]	15.3 (1.9)[a]
R_{merge}	0.068 (0.463)[a]	0.092 (0.435)[a]	0.094 (0.328)[a]	0.060 (0.248)[a]	0.074 (0.565)[a]	0.065 (0.601)[a]
	Crystals and Unit Cells					
space group	$P4_12_12$	$P4_12_12$	$P4_12_12$	$P4_12_12$	$P4_12_12$	$P4_12_12$
unit cell parameters						
$a = b$ (Å)	119.73	120.61	118.74	118.85	120.55	120.40
c (Å)	153.53	151.13	149.28	151.55	150.56	149.84
$\alpha = \beta = \gamma$ (deg)	90.00	90.00	90.00	90.00	90.00	90.00
	Refinement					
R_{work}	0.292	0.281	0.300	0.302	0.290	0.259
R_{free}[b]	0.335	0.346	0.355	0.333	0.357	0.299
rmsd for bond lengths (Å)	0.009	0.011	0.011	0.010	0.009	0.008
rmsd for bond angles (deg)	1.304	1.527	1.580	1.457	1.331	1.319
	Occupancy					
site 1	0.96	0.59	0.71	0.74	1.00	0.61
site 2	0.80	0.82	0.98	0.68	0.89	0.39
site 3	0.73	0.70	0.78	0.58	0.69	0.53
site 4	0.61	0.64	0.86	0.52	0.69	0.56
site 5	0.60	0.46	0.41	0.56	0.55	−
site 6	0.27	−	−	−	−	0.36
site 7	0.32	−	−	−	−	−

[a] Values in parentheses apply to the highest-resolution shell. [b] R_{free} is the R_{factor} based on 5% of the data excluded from refinement.

The locations of the Xe binding sites describe a continuous, bifurcated channel that opens from two points on the protein exterior, converges within subunit I, and leads directly to Cu_B of the dnc (Figure 1C,D). The entrance points face the bilayer 16 Å from the periplasmic side of the transmembrane domain, which is approximately one-third of the membrane thickness. The Y shape of the channel lies roughly parallel with the plane of the bilayer with its base opening directly into the heme a_3−Cu_B active site; Cu_B is ∼8 Å from Xe1. One arm of the Y terminates at Xe2 ∼20 Å from Cu_B, and the other arm terminates at Xe4, which is slightly recessed from the protein surface and ∼18 Å from Cu_B. In terms of relative occupancy, the highest-affinity site is at the base of the Y nearest the active site (Xe1); two of the next most occupied sites lie at the ends of the arms (Xe2 and Xe4), while Xe3, Xe5, and Xe7 are interior and roughly define the fork of the Y. Within the channel, the Xe sites are contiguous, i.e., although Xe−Xe interatomic distances are slightly greater than van der Waals contacts (range of 4.69–8.28 Å, except for one minor site at 3.27 Å), but there is insufficient space for any intervening sites. The channel is therefore defined by a series of proximate binding sites.

With respect to the fold of subunit I, the channel is bounded by transmembrane helices I-1–I-6, heme a_3, and heme b (Figure 1C,D). The branches of the Y are separated by the tightly packed pair of helices I-3 and I-4; the greater spacing of helices I-1 and I-2, and I-5 and I-6, on either side of this pair creates the arms and the stem of the Y. The upper surface of the Y is defined by the loop linking helices I-3 and I-4, which isolates the channel from the periplasmic facing surface of subunit I. The amino acid side chains lining the channel and surrounding the Xe binding sites are hydrophobic, as observed in other Xe- and Kr-derivatized proteins (*16*). All residues with van der Waals contacts to Xe atoms (≤5 Å) are listed in Table 1S of the Supporting Information. When sites are compared, there is no preference for specific amino acids or side chain type (aliphatic or aromatic), nor does the number of contacts at each site correlate with Xe occupancy. Nevertheless, it is interesting to note that Xe1, closest to the dnc cavity between Fe_{a3} and Cu_B, has van der Waals contacts with I-Tyr133, I-Phe228, I-Trp229, I-Trp239, I-Ile235, and one atom of the heme a_3 macrocycle (see Table 1S of the Supporting Information).

Difference Fourier maps following rigid body refinement revealed no significant backbone or side chain movements observed upon binding Xe or Kr atoms, suggesting that the cavity is relatively inflexible upon occupation by a noble gas. Indeed, if the van der Waals diameter of Xe is taken into account, each Xe atom fits snugly into its binding site. In other words, the Xe-pressurized and the native proteins are isomorphous, so an important characteristic of the hydrophobic channel is its presence in the native enzyme. Consequently, we rendered the channel boundaries of the Xe-bound structure using VOIDOO (*33*) (Figure 1C,D). With respect to the Xe-occupied protein, the channel has a volume of ∼390 $Å^3$, slightly smaller than the combined volume of

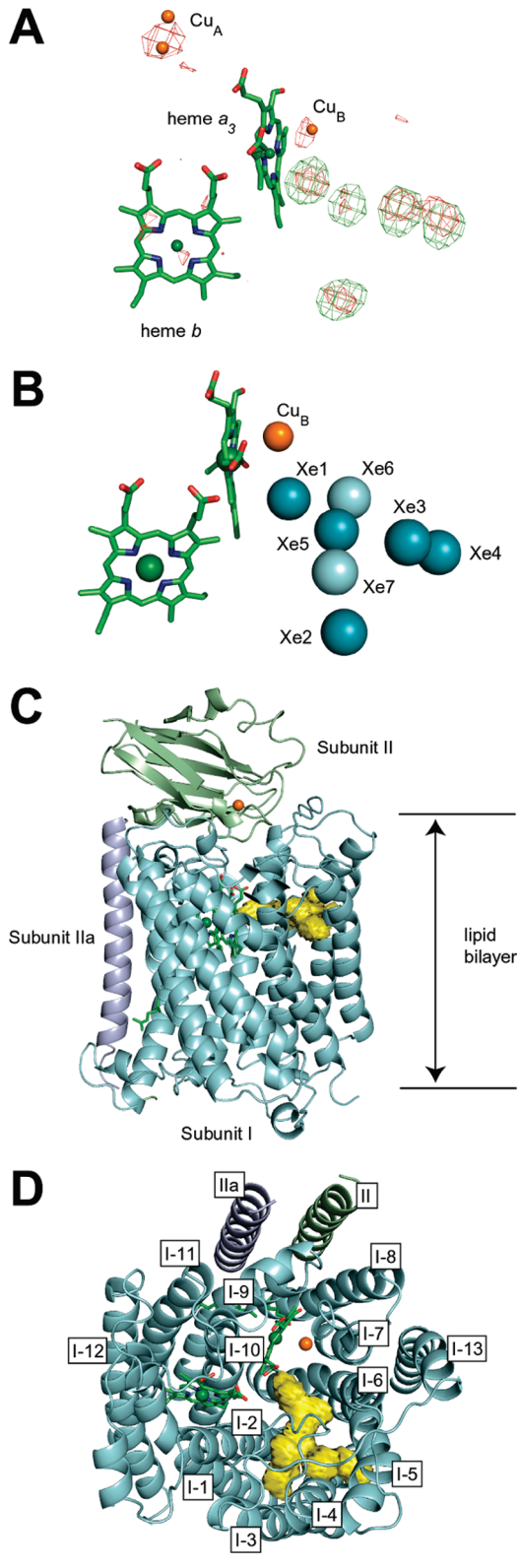

FIGURE 1: Xenon and channel locations. (A) Colored green is the $F_o - F_c$ map (6σ) of the ba_3 crystal pressurized for 5 min at 100 psi. Overlaid in red is the $F^+ - F^-$ map (5σ) of the same crystal confirming the presence and locations of Fe, Cu, and Xe. (B) Locations of the major (teal) and minor (light teal) Xe sites following refinement against the data set in panel A. Sites were numbered from highest to lowest occupancy in the 3.37 Å resolution data set (Table 1). (C) Transmembrane view of ba_3 illustrating the location of the computationally derived oxygen channel (yellow). (D) Top view of ba_3 showing the Y shape of the channel. Helix 4 of subunit I bisects the two arms of the channel.

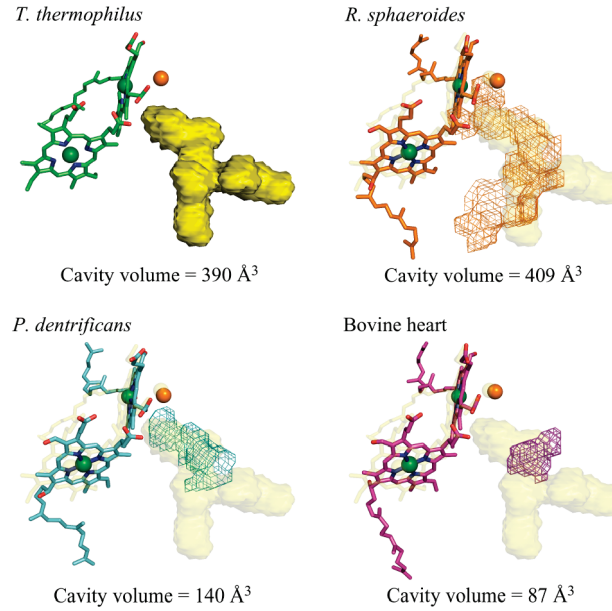

FIGURE 2: Hydrophobic channels and volumes of cytochrome *c* oxidases with known structures. Cytochrome ba_3 oxidase from *T. thermophilus* (yellow surface in all panels) is the only channel with a Y shape. The structure of each cytochrome *c* oxidase was superimposed onto ba_3 to allow comparison of channels. Each channel (wire rendition) was then overlaid on the ba_3 channel. Although the *R. sphaeroides* cytochrome *c* oxidase channel has a larger volume than ba_3, it only has one entry point. Channels from *P. denitrificans* and bovine heart cytochrome *c* oxidase have significantly smaller volumes and do not bridge their respective enzymatic centers to the outside of each protein. All four channels appear to share the volume occupied by site 3 (Figure 1B). The orange sphere is Cu_B in each panel.

seven Xe atoms (406 Å^3); a calculation with FLOOD (*33*) shows that no more than eight Xe atoms can fit into this volume, which is roughly consistent with eight Xe atoms that have a combined volume of 464 Å^3.

Cavities were assessed within the three other cytochrome *c* oxidases with available structures: *Rs* (PDB entry 1M56) (*7*), *Pd* (PDB entry 1AR1) (*5*), and bovine heart (PDB entry 1OCC) (*4*). The computed voids were superimposed onto the cytochrome ba_3 channel via superposition of the protein structures, illustrating that the putative O_2 pathway is a conserved feature, albeit with greatly varying geometry (Figure 2). The channel in *Rs* has a larger volume (409 Å^3) than ba_3 but only one entry point; this channel also encompasses the two observed Xe sites (*7*). In contrast, the cavities within the *Pd* and bovine heart structures are truncated and not connected to the protein surface, although the partial channel in *Pd* adjoins the enzymatic center having a potential site similar to that of Xe1 in ba_3. Because the channels or cavities superpose, we performed secondary structure-based sequence alignment (*32*) (Figure 3). The residues and helices lining the channels exhibit marked sequence and structural similarity in all four cytochrome *c* oxidases, even though ba_3 is a divergent member of the family (*34*). This alignment supports the coincidence of channels and cavities (Figure 2) in sequence space.

The large voids in these proteins contain no bound H_2O molecules in high-resolution structures of the native enzymes (PDB entries 1XME, 1EHK, and 2GSM). Hydrophobic cavities in water soluble proteins, surrounded by ~55 M water, have been shown to contain fixed water molecules at

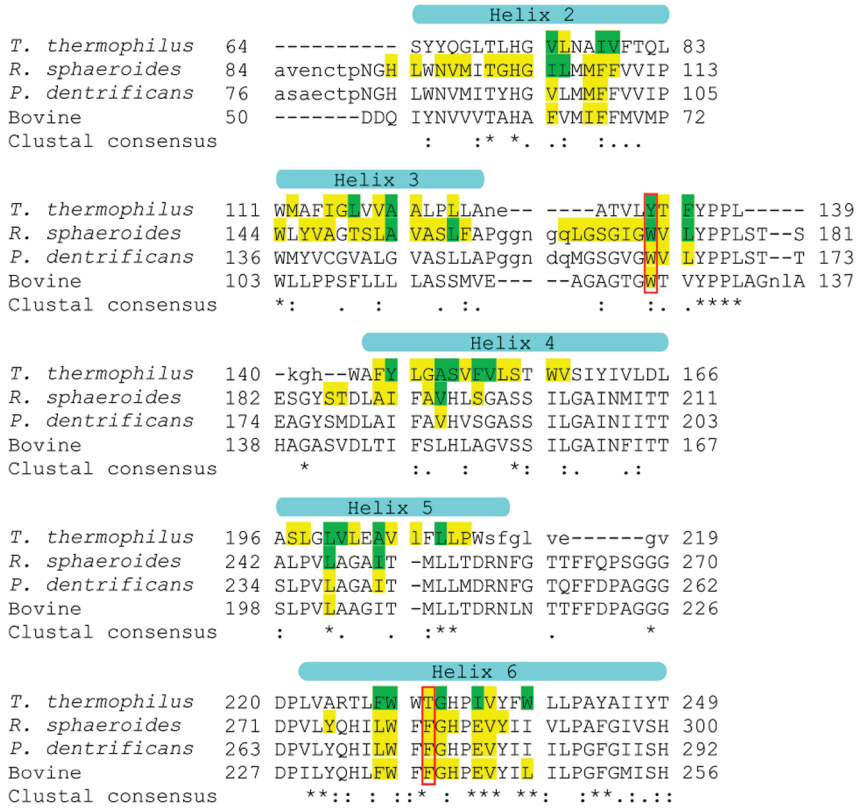

FIGURE 3: Structure and sequence homology. Shown are selected stretches of residues from a structure-based alignment of the four cytochrome *c* oxidases. In capital letters are residues that share similar atomic coordinates when the cytochrome *c* oxidases are superposed. The consensus line shows sequence homology as follows: asterisk, fully conserved; colon, strong group conservation; and period, conserved weak groups as defined in ClustalW. Colored yellow are all the residues that line the putative oxygen channels (Figure 2), and colored green are the residues that have been shown to be in contact with xenon atoms where these experiments have been conducted, e.g., Table 1S. All the residues highlighted in green were also found in the computational channel search. Highlighted in the red boxes are the residues that form the constriction point found in all cytochrome *c* oxidases that were investigated, except ba_3 (see the text) (cyan bars, secondary structure elements).

high pressures (*35*). The amino acid residues within the interior of proteins are thought to be packed like crystals of small organic molecules (*36*). The presence of a large void in a protein, presumably supporting a vacuum, is generally thought to lower its thermodynamic stability (*37*).

The Xe-derivatized structure of cytochrome *c* oxidase from *Rs* also revealed a possible oxygen pathway (*7*) (Figure 2). On the basis of these studies, a single mutation of Gly to Val (I-283, *Rs*) was shown to obstruct the passageway of oxygen and render the enzyme inactive (*38*). The oxygen channel in *Ec* bo_3 was deduced by visualization, and a mutation (Val287 to Ile287, *Ec*) decreased the rate of O_2 consumption by raising $K_{M,app}$ 10−15-fold (*21*). Examinations of the cytochrome *c* oxidases from *Pd* and bovine heart do not reveal clearly distinguishable hydrophobic channels to their respective dncs (Figure 2). However, kinetic data presented by Riistima et al. suggest that oxygen approaches the enzymatic center of *Pd* cytochrome *c* oxidase without hindrance from protein residues (*21*), suggesting that side chain mobility may also be important in O_2 uptake.

As with all heme copper oxidases, one function of ba_3 is proton translocation. Data from enzymes of the A1 type have converged to reveal that one proton is pumped out for each electron received from cytochrome *c*, and ba_3 is likely not to differ in this respect.[2] In A1-type enzymes (*34*), both electron transfer and proton pumping activities have been shown to be strongly dependent on the conserved Glu (Glu286 in *Rs* and *Ec*, Glu278 in *Pd*, and Glu242 in bovine heart) (see ref *41* and references therein). Interestingly, the isopositional residue in *Tt* ba_3 is I-Ile235; this also holds for the A2-type enzymes, e.g., caa_3 from *Tt*. The methyl group (CG2) of I-Ile235 in ba_3 is close to Xe1, 3.96 Å, and the torsion angles of the side chain appear optimized to make this group part of the surface of the O_2 channel. In the structures of the A1-type enzymes, the carboxyl group of this glutamate points away from the O_2 channel, while atoms CB and CG (corresponding to the CB and CG atoms of I-Ile235, respectively) form part of the surface of the O_2 channel in this region. Our structures support a claim for a role of the Glu residue at this position in maintaining the O_2 channel (*9*).

[2] Kaant et al. (*39*) reported in 1998 that the number of protons pumped per electron transferred to O_2 from cytochrome *c* (H^+/e^-) by *Tt* cytochrome ba_3 is 0.5, and Konstantinov et al. (*40*) have rationalized their mechanistic results with this number in mind. However, almost certainly this value is low. M. Wikström (unpublished personal communication), working with protein obtained from this laboratory, found an H^+/e^- value of 0.7, and one can expect this ratio to approach the canonical value of 1 as more experience is gained with the enzyme.

DISCUSSION

The structures presented here are relevant to the rate and mechanism via which atmospheric O_2 gains access to the $Fe(II)_{a3}-Cu_B(I)$ dnc of cytochrome *c* oxidases, interaction of CO with *ba*$_3$, pathways via which O_2 enters and H_2O leaves the dnc, and the role of the oxygen channel in the thermophilicity of *T. thermophilus*.

Rate and Mechanism of O$_2$ *Binding.* The interaction of O_2 with heme a_3 has been the object of physiological studies for many years. In general, oxygen consumption by various aerobic tissues is kinetically zero-order in oxygen down to very low O_2 concentrations, whereupon apparent Michaelis–Menten kinetics prevail (*42*). Typical values of $K_{M,app}$, obtained from V_{max} (O_2 consumed per a_3 per second)/$k_1[a_3]_{tot}$, are on the order of 50×10^{-9} M O_2. Here k_1 corresponds to the observed second-order rate constant for the reaction of aqueous O_2 with reduced heme a_3, and $[a_3]_{tot}$ corresponds to the molar concentration of enzyme. Notably, k_1 shows little variation with different types of tissues, being $\sim 10^8$ M^{-1} s^{-1}, indicating that the reaction is diffusion-controlled.

Uptake of oxygen by the dnc has been widely studied by rapid-kinetic, flow-flash experiments at ambient temperature (see ref *43* for a review), and at sub-zero temperatures using "triple trap" (*44*), and the results are relevant to the interpretation of our structures. The first observable intermediate in the catalytic cycle is an oxy complex, $Fe_{a_3}^{2+}-O_2$. The actual affinity of O_2 for heme a_3, however, is quite weak, $\sim 10^{-3}$ M. The extremely low $K_{M,app}$ is thus likely due to electron transfer from the low-spin heme to the dnc, resulting in the irreversible binding of O_2 (*44, 45*). In discussing this phenomenon in *Ec bo*$_3$, Riistama et al. (*21*) suggest that $K_{M,app}$ will vary proportionally with the rate of O_2 diffusion, provided that the rate of O_2 trapping by electron transfer is faster than the off-rate from the oxy complex. These authors suggest a modified expression for $K_{M,app} = \sim k_{et}/k_1K_D$, where k_{et} is the rate constant for electron transfer from the low-spin heme to the dnc, thereby trapping O_2; K_D is the true dissociation constant for the reaction between O_2 and the high-spin heme (o_3 in the case of the homologous *Ec bo*$_3$) in which there is no trapping reaction; and k_1 is, as described above, the diffusion-controlled rate constant for the reaction of the high-spin heme with O_2. Hence, the value of k_1 contains information about the processes via which O_2 reaches the dnc.

Relevant to this work is the generally held belief that diffusion of O_2 through tissues occurs to a significant extent within lipid bilayers. One foundation of this idea is that oxygen concentrates within the hydrophobic interior of fluid lipid membranes because it is more soluble in organic solvents than in water; for example, a reasonable distribution of O_2 from water into biological membranes is $\sim 4-5$ (*46*). It is also generally held that solubilization of O_2 requires the presence of either fixed or dynamic "holes" where the O_2 molecule can insert itself. This was elegantly demonstrated for hydrophobic materials by Kimmich and Peters (*47*), who showed that samples of crystalline paraffins, e.g., n-$C_{19}H_{40}$, contain no O_2. However, when warmed, oxygen penetrates the paraffins. Similar observations have been made with fluid and ordered or frozen bilayer preparations (*48*). It is therefore reasonable to think of the individual Xe-binding sites in *ba*$_3$'s oxygen channel as rigid holes within which oxygen molecules may momentarily collect prior to entering the dnc.

Direct evidence that O_2 enters the lipid bilayer and diffuses therein was obtained by Vanderkooi and co-workers (*46, 49*). Magnetic resonance methods have been described (*50*) that measure the diffusion solubility product, $D_T[O_2]$, in membranes, where D_T is the diffusion constant of O_2 at a given temperature (centimeters per square second) and $[O_2]$ is the molar O_2 concentration in the neighborhood of the probe molecule ($D_T[O_2]$ is termed the oxygen permeation coefficient). Position-specific, spin-labeled fatty acid nitroxides have made it possible to measure this coefficient at unique positions along the normal to the lipid bilayer. These studies (*48, 50, 51*) reveal a Gaussian sigmoidal shape of $D_T[O_2]$ versus position on the normal that is called the oxygen permeation profile. The value of $D_T[O_2]$ is lowest near the periphery and has its maximum at the center of the bilayer. Transport of O_2 to the dnc thus depends on the values of $D_T^{H_2O}[O_2]$, $D_T^{lipid}[O_2]$, and $D_T^{channel}[O_2]$ from which the importance of both D_T and local $[O_2]$ is evident. Notably, the entryways to the O_2 channel in cytochrome *ba*$_3$ and those of other oxidases are located approximately two-thirds of the distance from the outer surface to the center of the membrane, thereby placing them near the point of most efficient oxygen delivery. By contrast, the permeation profile of water is the opposite of that of oxygen, being lowest at the center of the bilayer (*52*) and thereby reflecting water's greater polarity and offering an at least partial explanation for the crystallographic absence of water in oxygen channels (*4–9*).

Interaction of CO with ba$_3$*.* As shown in Figure 2, the oxygen channels of bovine *aa*$_3$ and *ba*$_3$ overlap to some degree, but that of the bovine enzyme is $\sim$4.5-fold smaller in volume and extends neither into the bilayer space nor into the dnc. The details of O_2 transport by the bovine enzyme must differ greatly from those for *ba*$_3$. Indeed, these structural differences may cause their disparate CO binding properties. Carbon monoxide has long been recognized as an appropriate analogue for the study of O_2 binding to heme proteins (*53*). CO has the desirable properties of binding to heme Fe, but generally not undergoing further reactions, as does Fe-bound O_2, and CO possesses infrared absorption properties that permit spectroscopic probing of its immediate environment (see below).

There have been numerous, detailed comparisons of the interactions of CO with bovine *aa*$_3$ and *ba*$_3$ (*54–56*) [see Table 1 of Woodruff (*56*)]. The data are generally treated (ignoring photochemical events) by two linked equilibria

$$CO + \{Fe_{a_3}^{2+}, Cu_B^{+}\} \underset{K_1}{\longrightarrow} \{Fe_{a_3}^{2+}, Cu_B^{+}-CO\} \underset{K_2}{\longrightarrow} \{Fe_{a_3}^{2+}-CO, Cu_B^{+}\}$$

where $K_1 = k_1[CO]/k_{-1}$ (M^{-1}) and $K_2 = k_2/k_{-2}$. There are two remarkable differences between these enzymes. First, the affinity constant, K_1, of *ba*$_3$ is $\sim$115-fold greater than the K_1 for the bovine enzyme, a difference that may be reasonably associated with a higher local CO concentration available to the dnc in *ba*$_3$. Second, the affinity constant, K_2, of *ba*$_3$ is $\sim$3000-fold smaller than the K_2 for the bovine

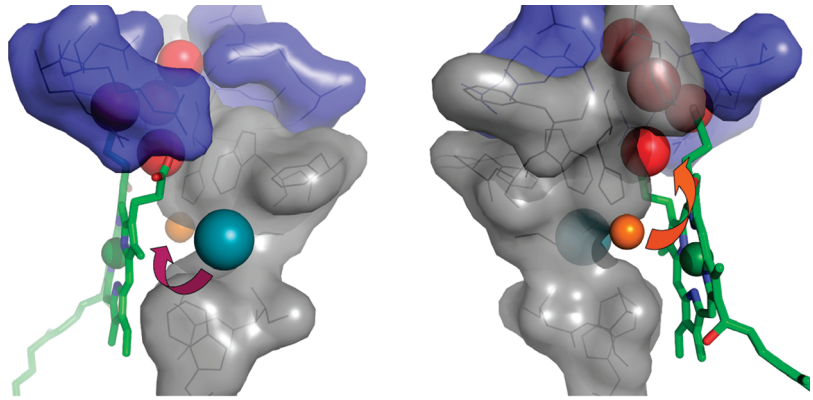

FIGURE 4: Hydrophobic−hydrophilic boundary around the dinuclear center (left and right images are 180° rotations of each other). Surface renditions of the pocket encompassing the dinuclear center are primarily hydrophobic (gray). Shown on the left, Trp229 and His283 impede direct access from the Xe1 site (slate) to the Cu_B (orange) of the dinuclear center (purple arrow). This primarily hydrophobic trajectory is ideal for oxygen access (left panel). We hypothesize that after the conversion of O_2 to H_2O, the H_2O exits the dinuclear center through a region occupied by hydrophilic amino acids (surface representation colored blue) between the propionates of heme a_3 (orange arrow, right panel). Although not present in our structures, ordered waters (red) found at the heme a_3 propionates based on a higher-resolution ba_3 structure (PDB entry 1XME) are depicted.

enzyme, a difference that is unlikely related to differences in the two oxygen channels.

Varotsis and co-workers (*57, 58*) have expanded the scope of CO−ba_3 interactions by utilizing the technique of time-resolved, step-scan FTIR spectroscopy with samples at ambient temperature. These reveal changes in the vibrational properties of both the protein itself and those of protein-bound CO. To briefly summarize, flash photolysis of fully reduced, carbonylated ba_3 results in direct conversion from $Fe_{a_3}^{2+}$−CO to Cu_B^{+}−CO in ~80% of the enzyme molecules. In the remaining ~20% of the photolyzed $Fe_{a_3}^{2+}$−CO molecules, CO migrates to a nonmetal site and vCO appears instantaneously at 2131 cm^{-1} (*58*). The residence time of CO in this position is ~60 μs, from which it returns to neither $Fe_{a_3}^{2+}$ nor Cu_B^{+} but becomes spectroscopically silent. Concomitant with the immediate appearance and disappearance over ~60 μs of the 2131 cm^{-1} band is the return of a carbonyl (C═O) stretching band, following photolysis, at 1702 cm^{-1} to the relaxed C═O band at 1708 cm^{-1}. Two critical assignments are made in the interpretation of these observations. (a) The non-Cu-bound CO is close to the heme (*58*), and (b) the changes in the 1702−1708 cm^{-1} range arise from the perturbation of the C═O stretching of a propionate carbonyl, specifically that on ring A of heme a_3.

Our structural observations of the Xe1 site suggest that that portion of the activated CO that does not bind to Cu_B finds its way to the Xe1 site where it may interact weakly with the heme methyl group on ring A and with the CBA atom of the propionate side chain of ring A, resulting in a perturbation of the propionate C═O stretch. These groups are, respectively, 5.1 and 4.9 Å from the Xe1 atom in our structures. Migration of this CO molecule farther into the channel would likely result in loss of spectroscopic signature. Similar ideas might be applied to the studies of the Varotsis group of oxygen-linked interactions of CO with ba_3 (*59*).

Entrance and Exit Pathways for O_2 and H_2O. On the basis of its location, the Xe1 site serves as the portal into the dnc for O_2. Previous studies have suggested that CO and O_2 initially bind to Cu_B before being transferred to heme a_3 (*60*). However, there is no evidence for the thermal population of a Cu_B−CO species. Moreover, there is no straight-line access from the Xe1 site to Cu_B; Trp229 and His283 form a "wall" which O_2 needs to circumvent before entering the dnc (Figure 4). This environment, where connected to the channel, is primarily hydrophobic and lined by the following residues: Trp229, Gly232, His233, Ile235, Val236, Trp239, Phe281, His282, His283, and Phe285. Although O_2 favors this hydrophobic environment, during enzymatic turnover, the H_2O produced does not. Further, H_2O must leave the dnc before O_2 can enter. We hypothesize that the newly formed H_2O molecules are repelled by the hydrophobic surface of the O_2 channel but attracted to the hydrophilic area around the heme a_3 propionates where they exit the dnc (Figure 4). This hydrophilic "vent" is composed of the following: Arg225, Gln284, Asp287, Asp372, Asn377, Arg449, and Arg350. Although they are not present in our Xe-derivatized structures, the high-resolution structures of ba_3 (PDB entries 1XME and 1EHK) reveal ordered waters at the heme a_3 propionates (*8, 9*). These waters lead to a pool of waters between subunit I and the periplasmic domain of subunit II and are highly conserved in other cytochrome *c* oxidase structures (*4–9*). Partitioning of O_2 and H_2O between the two environments surrounding the dnc is consistent with diffusion of CO back into the Xe1 site, as noted above. Further, spatially separated vectorial transfer from substrate (O_2) to product (H_2O) cavities during turnover would increase the overall rate of the reaction.

Access to the Dinuclear Center in Other Cytochrome c Oxidases. If we consider the dimensions of both the ba_3 channel and molecular oxygen, O_2 would have no obstruction to accessing the a_3−Cu_B center. In comparison, the other cytochrome *c* oxidases with known structures do not have this feature. The *Rs* aa_3 has a hydrophobic channel (Figure 2), but it has a constriction point, which reduces the channel diameter. This occurs at Trp172 and Phe282 (*Rs* numbering), where the surface-to-surface distance of these residues reduces the diameter of the channel to 1.7 Å, which would restrict passage of an O_2 molecule (Figure 5). The residues forming this constriction point in *Rs* are conserved in both *Pd* and bovine heart (Figure 3). Presumably in these oxidases, some protein motion or rearrangement needs to occur for oxygen to have access to their respective enzymatic centers.

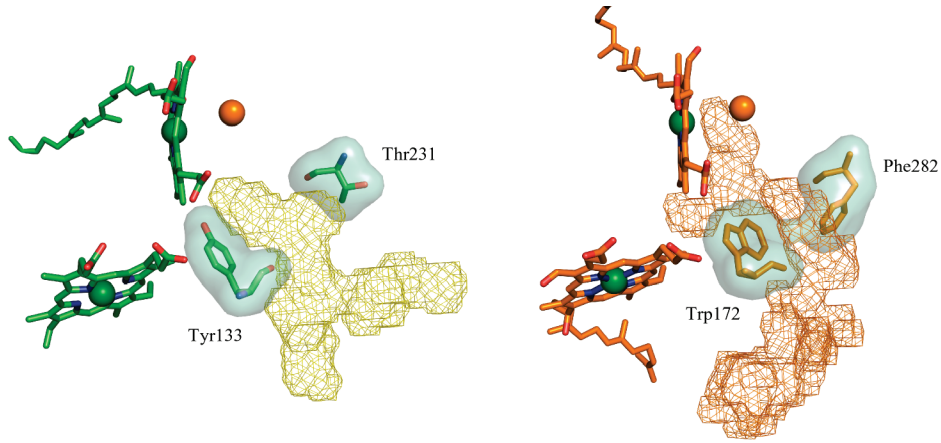

FIGURE 5: Oxygen access to the enzymatic center. For *R. sphaeroides*, *P. denitrificans*, and bovine heart cytochrome *c* oxidases (only *R. sphaeroides* is shown), there is a constriction point where the channel narrows and does not allow access to the enzymatic center without some conformational change occurring. These residues are conserved (refer to Figure 3), except in the case of ba_3. The channel of ba_3 does not share this narrowing feature.

On the other hand, ba_3 does not share these conserved residues, containing the smaller Tyr133 and Thr231 residues instead (Figures 3 and 5), and therefore lacks a channel narrowing (Figure 4).

Thermus Physiology. The optimum growth temperature of *T. thermophilus* HB8 (*2*) is 70 °C, where air-saturated water contains approximately half the amount of O_2 as water at 25 °C. In light of the above discussion regarding the mechanisms for transport of O_2 from the atmosphere into the dnc of ba_3 and by virtue of its extreme hydrophobic and rigid binding sites for Xe (O_2) molecules, it is reasonable to speculate that the continuous, Y-shaped oxygen channel of ba_3 actively facilitates transfer of O_2 from the membrane into the dnc, and that it was sculpted by and remains subject to the forces of natural selection. Our structures are a springboard for elucidating further details of ligand migration within a cytochrome *c* oxidase.

ACKNOWLEDGMENT

Portions of this research were carried out at the Stanford Synchrotron Radiation Laboratory, a national user facility operated by Stanford University on behalf of the U.S. Department of Energy, Office of Basic Energy Sciences. The SSRL Structural Molecular Biology Program is supported by the Department of Energy, Office of Biological and Environmental Research, and by the National Institutes of Health, National Center for Research Resources, Biomedical Technology Program, and the National Institute of General Medical Sciences. We thank the support staff of SSRL for generous assistance.

SUPPORTING INFORMATION AVAILABLE

A table of residues in contact with the xenon atoms (Table 1S). This material is available free of charge via the Internet at http://pubs.acs.org.

REFERENCES

1. Ferguson-Miller, S., and Babcock, G. T. (1996) Heme/Copper Terminal Oxidases. *Chem. Rev. 96*, 2889–2908.
2. Oshima, T., and Imahori, K. (1974) Description of *Thermus thermophilus* Comb-Nov, a nonsporulating thermophilic bacterium from a Japanese thermal spa. *Int. J. Syst. Bacteriol. 24*, 102–112.
3. Zimmermann, B. H., Nitsche, C. I., Fee, J. A., Rusnak, F., and Munck, E. (1988) Properties of a copper-containing cytochrome ba_3: A second terminal oxidase from the extreme thermophile *Thermus thermophilus*. *Proc. Natl. Acad. Sci. U.S.A. 85*, 5779–5783.
4. Tsukihara, T., Aoyama, H., Yamashita, E., Tomizaki, T., Yamaguchi, H., Shinzawa-Itoh, K., Nakashima, R., Yaono, R., and Yoshikawa, S. (1996) The whole structure of the 13-subunit oxidized cytochrome c oxidase at 2.8 Å. *Science 272*, 1136–1144.
5. Iwata, S., Ostermeier, C., Ludwig, B., and Michel, H. (1995) Structure at 2.8 Å resolution of cytochrome c oxidase from *Paracoccus denitrificans*. *Nature 376*, 660–669.
6. Qin, L., Hiser, C., Mulichak, A., Garavito, R. M., and Ferguson-Miller, S. (2006) Identification of conserved lipid/detergent-binding sites in a high-resolution structure of the membrane protein cytochrome c oxidase. *Proc. Natl. Acad. Sci. U.S.A. 103*, 16117–16122.
7. Svensson-Ek, M., Abramson, J., Larsson, G., Tornroth, S., Brzezinski, P., and Iwata, S. (2002) The X-ray crystal structures of wild-type and EQ(I-286) mutant cytochrome c oxidases from *Rhodobacter sphaeroides*. *J. Mol. Biol. 321*, 329–339.
8. Hunsicker-Wang, L. M., Pacoma, R. L., Chen, Y., Fee, J. A., and Stout, C. D. (2005) A novel cryoprotection scheme for enhancing the diffraction of crystals of recombinant cytochrome ba_3 oxidase from *Thermus thermophilus*. *Acta Crystallogr. D61*, 340–343.
9. Soulimane, T., Buse, G., Bourenkov, G. P., Bartunik, H. D., Huber, R., and Than, M. E. (2000) Structure and mechanism of the aberrant ba_3-cytochrome c oxidase from *Thermus thermophilus*. *EMBO J. 19*, 1766–1776.
10. Abramson, J., Riistama, S., Larsson, G., Jasaitis, A., Svensson-Ek, M., Laakkonen, L., Puustinen, A., Iwata, S., and Wikstrom, M. (2000) The structure of the ubiquinol oxidase from *Escherichia coli* and its ubiquinone binding site. *Nat. Struct. Biol. 7*, 910–917.
11. Babcock, G. T., and Wikstrom, M. (1992) Oxygen activation and the conservation of energy in cell respiration. *Nature 356*, 301–309.
12. Farver, O., Chen, Y., Fee, J. A., and Pecht, I. (2006) Electron transfer among the CuA-, heme b- and a_3-centers of *Thermus thermophilus* cytochrome ba_3. *FEBS Lett. 580*, 3417–3421.
13. Cohen, J., Arkhipov, A., Braun, R., and Schulten, K. (2006) Imaging the migration pathways for O-2, CO, NO, and Xe inside myoglobin. *Biophys. J. 91*, 1844–1857.
14. Soltis, S. M., Stowell, M. H. B., Wiener, M. C., Phillips, G. N., and Rees, D. C. (1997) Successful flash-cooling of xenon-derivatized myoglobin crystals. *J. Appl. Crystallogr. 30*, 190–194.
15. Schoenborn, B. P. (1965) Binding of xenon to horse haemoglobin. *Nature 208*, 760–762.
16. Prange, T., Schiltz, M., Pernot, L., Colloc'h, N., Longhi, S., Bourguet, W., and Fourme, R. (1998) Exploring hydrophobic sites in proteins with xenon or krypton. *Proteins 30*, 61–73.
17. Sawyer, D. T., Chlericato, G., Angelis, C. T., Nanni, E. J., and Tsuchiya, T. (1982) Effects of media and electrode materials on the electrochemical reduction of dioxygen. *Anal. Chem. 54*, 1720–1724.

18. Bondi, A. (1964) van der Waals volumes and radii. *J. Phys. Chem. 68*, 441–451.
19. Bader, R. F. W., Henneker, W. H., and Cade, P. E. (1967) Molecular charge distributions and chemical binding. *J. Chem. Phys. 46*, 3341.
20. Hofacker, I., and Schulten, K. (1998) Oxygen and proton pathways in cytochrome c oxidase. *Proteins 30*, 100–107.
21. Riistama, S., Puustinen, A., Garcia-Horsman, A., Iwata, S., Michel, H., and Wikstrom, M. (1996) Channelling of dioxygen into the respiratory enzyme. *Biochim. Biophys. Acta 1275*, 1–4.
22. Liu, B., Luna, V. M., Chen, Y., Stout, C. D., and Fee, J. A. (2007) An unexpected outcome of surface engineering an integral membrane protein: Improved crystallization of cytochrome ba_3 from *Thermus thermophilus*. *Acta Crystallogr. F63*, 1029–1034.
23. Chen, Y., Hunsicker-Wang, L., Pacoma, R. L., Luna, E., and Fee, J. A. (2005) A homologous expression system for obtaining engineered cytochrome ba_3 from *Thermus thermophilus* HB8. *Protein Expression Purif. 40*, 299–318.
24. Leslie, A. G. (1999) Integration of macromolecular diffraction data. *Acta Crystallogr. D55*, 1696–1702.
25. Collaborative Computational Project Number 4 (1994) The CCP4 suite: programs for protein crystallography. *Acta Crystallogr. D50*, 760–763.
26. Emsley, P., and Cowtan, K. (2004) Coot: Model-building tools for molecular graphics. *Acta Crystallogr. D60*, 2126–2132.
27. Murshudov, G. N., Vagin, A. A., and Dodson, E. J. (1997) Refinement of macromolecular structures by the maximum-likelihood method. *Acta Crystallogr. D53*, 240–255.
28. Painter, J., and Merritt, E. A. (2006) Optimal description of a protein structure in terms of multiple groups undergoing TLS motion. *Acta Crystallogr. D62*, 439–450.
29. Brunger, A. T., Adams, P. D., Clore, G. M., DeLano, W. L., Gros, P., Grosse-Kunstleve, R. W., Jiang, J. S., Kuszewski, J., Nilges, M., Pannu, N. S., Read, R. J., Rice, L. M., Simonson, T., and Warren, G. L. (1998) Crystallography & NMR system: A new software suite for macromolecular structure determination. *Acta Crystallogr. D54*, 905–921.
30. McPhillips, T. M., McPhillips, S. E., Chiu, H. J., Cohen, A. E., Deacon, A. M., Ellis, P. J., Garman, E., Gonzalez, A., Sauter, N. K., Phizackerley, R. P., Soltis, S. M., and Kuhn, P. (2002) Blu-Ice and the Distributed Control System: Software for data acquisition and instrument control at macromolecular crystallography beamlines. *J. Synchrotron Radiat. 9*, 401–406.
31. Thompson, J. D., Higgins, D. G., and Gibson, T. J. (1994) CLUSTAL W: Improving the sensitivity of progressive multiple sequence alignment through sequence weighting, position-specific gap penalties and weight matrix choice. *Nucleic Acids Res. 22*, 4673–4680.
32. Bruns, C. M., Hubatsch, I., Ridderstrom, M., Mannervik, B., and Tainer, J. A. (1999) Human glutathione transferase A4-4 crystal structures and mutagenesis reveal the basis of high catalytic efficiency with toxic lipid peroxidation products. *J. Mol. Biol. 288*, 427–439.
33. Kleywegt, G. J., and Jones, T. A. (1994) Detection, delineation, measurement and display of cavities in macromolecular structures. *Acta Crystallogr. D50*, 178–185.
34. Pereira, M. M., Santana, M., and Teixeira, M. (2001) A novel scenario for the evolution of haem-copper oxygen reductases. *Biochim. Biophys. Acta 1505*, 185–208.
35. Collins, M. D., Hummer, G., Quillin, M. L., Matthews, B. W., and Gruner, S. M. (2005) Cooperative water filling of a nonpolar protein cavity observed by high-pressure crystallography and simulation. *Proc. Natl. Acad. Sci. U.S.A. 102*, 16668–16671.
36. Richards, F. M. (1974) The interpretation of protein structures: Total volume, group volume distributions and packing density. *J. Mol. Biol. 82*, 1–14.
37. Lee, B. (1993) Estimation of the maximum change in stability of globular proteins upon mutation of a hydrophobic residue to another of smaller size. *Protein Sci. 2*, 733–738.
38. Salomonsson, L., Lee, A., Gennis, R. B., and Brzezinski, P. (2004) A single-amino-acid lid renders a gas-tight compartment within a membrane-bound transporter. *Proc. Natl. Acad. Sci. U.S.A. 101*, 11617–11621.
39. Kannt, A., Soulimane, T., Buse, G., Becker, A., Bamberg, E., and Michel, H. (1998) Electrical current generation and proton pumping catalyzed by the ba_3-type cytochrome c oxidase from *Thermus thermophilus*. *FEBS Lett. 434*, 17–22.
40. Konstantinov, A. A., Siletsky, S., Mitchell, D., Kaulen, A., and Gennis, R. B. (1997) The roles of the two proton input channels in cytochrome c oxidase from *Rhodobacter sphaeroides* probed by the effects of site-directed mutations on time-resolved electrogenic intraprotein proton transfer. *Proc. Natl. Acad. Sci. U.S.A. 94*, 9085–9090.
41. Nyquist, R. M., Heitbrink, D., Bolwien, C., Gennis, R. B., and Heberle, J. (2003) Direct observation of protonation reactions during the catalytic cycle of cytochrome c oxidase. *Proc. Natl. Acad. Sci. U.S.A. 100*, 8715–8720.
42. Chance, B. (1965) Reaction of oxygen with respiratory chain in cells and tissues. *J. Gen. Physiol. 49*, 163–195.
43. Einarsdottir, O. (1995) Fast reactions of cytochrome oxidase. *Biochim. Biophys. Acta 1229*, 129–147.
44. Chance, B., Saronio, C., and Leigh, J. S. (1975) Functional intermediates in reaction of membrane-bound cytochrome-oxidase with oxygen. *J. Biol. Chem. 250*, 9226–9237.
45. Han, S., Ching, Y. C., and Rousseau, D. L. (1990) Cytochrome c oxidase: Decay of the primary oxygen intermediate involves direct electron transfer from cytochrome a. *Proc. Natl. Acad. Sci. U.S.A. 87*, 8408–8412.
46. Fischkoff, S., and Vanderkooi, J. M. (1975) Oxygen diffusion in biological and artificial membranes determined by the fluorochrome pyrene. *J. Gen. Physiol. 65*, 663–676.
47. Kimmich, R., and Peters, A. (1975) Solvation of oxygen in lechtin bilayers. *Chem. Phys. Lipids 14*, 350–362.
48. Peters, A., and Kimmich, R. (1978) Heterogeneous solubility of oxygen in aqueous lecithin dispersions and its relation to chain mobility: NMR relaxation and wide-line study. *Biophys. Struct. Mech. 4*, 67–85.
49. Wilson, D. F., Rumsey, W. L., Green, T. J., and Vanderkooi, J. M. (1988) The oxygen dpendence of mitochondrial oxidative phosphorylation measured by a new optical method for measuring oxygen concentration. *J. Biol. Chem. 263*, 2712–2718.
50. Kusumi, A., Subczynski, W. K., and Hyde, J. S. (1982) Oxygen transport parameter in membranes as deduced by saturation recovery measurements of spin-lattice relaxation times of spin labels. *Proc. Natl. Acad. Sci. U.S.A. 79*, 1854–1858.
51. Marsh, D., Dzikovski, B. G., and Livshits, V. A. (2006) Oxygen profiles in membranes. *Biophys. J. 90*, L49–L51.
52. Erilov, D. A., Bartucci, R., Guzzi, R., Shubin, A. A., Maryasov, A. G., Marsh, D., Dzuba, S. A., and Sportelli, L. (2005) Water concentration profiles in membranes measured by ESEEM of spin-labeled lipids. *J. Phys. Chem. B 109*, 12003–12013.
53. Frauenfelder, H., McMahon, B. H., and Fenimore, P. W. (2003) Myoglobin: The hydrogen atom of biology and a paradigm of complexity. *Proc. Natl. Acad. Sci. U.S.A. 100*, 8615–8617.
54. Fiamingo, F. G., Altschuld, R. A., Moh, P. P., and Alben, J. O. (1982) Dynamic interactions of CO with a_3Fe and CuB in cytochrome c oxidase in beef heart mitochondria studied by Fourier-transform infrared spectroscopy at low temperatures. *J. Biol. Chem. 257*, 1639–1650.
55. Giuffre, A., Forte, E., Antonini, G., D'Itri, E., Brunori, M., Soulimane, T., and Buse, G. (1999) Kinetic properties of ba_3 oxidase from *Thermus thermophilus*: Effect of temperature. *Biochemistry 38*, 1057–1065.
56. Woodruff, W. H. (1993) Coordination dynamics of heme-copper oxidases: The ligand shuttle and the control and coupling of electron transfer and proton translocation. *J. Bioenerg. Biomembr. 25*, 177–188.
57. Koutsoupakis, K., Stavrakis, S., Pinakoulaki, E., Soulimane, T., and Varotsis, C. (2002) Observation of the equilibrium Cu-B-CO complex and functional implications of the transient heme a_3 propionates in cytochrome ba_3-CO from *Thermus thermophilus*: Fourier transform infrared (FTIR) and time-resolved step-scan FTIR studies. *J. Biol. Chem. 277*, 32860–32866.
58. Koutsoupakis, C., Soulimane, T., and Varotsis, C. (2003) Ligand binding in a docking site of cytochrome c oxidase: A time-resolved step-scan Fourier transform infrared study. *J. Am. Chem. Soc. 125*, 14728–14732.
59. Koutsoupakis, C., Soulimane, T., and Varotsis, C. (2003) Docking site dynamics of ba_3-cytochrome c oxidase from *Thermus thermophilus*. *J. Biol. Chem. 278*, 36806–36809.
60. Lemon, D. D., Calhoun, M. W., Gennis, R. B., and Woodruff, W. H. (1993) The gateway to the active site of heme copper oxidases. *Biochemistry 32*, 11953–11956.

BI800045Y